Eur. Phys. J. B **42**, 51–61 (2004)
DOI: 10.1140/epjb/e2004-00357-8

THE EUROPEAN PHYSICAL JOURNAL B

Influence of oxygen vacancies on the magnetic and electrical properties of $La_{1-x}Sr_xMnO_{3-x/2}$ manganites

S.V. Trukhanov[1,a], L.S. Lobanovski[1], M.V. Bushinsky[1], V.A. Khomchenko[1], N.V. Pushkarev[1], I.O. Troyanchuk[1], A. Maignan[2], D. Flahaut[2], H. Szymczak[3], and R. Szymczak[3]

[1] Institute of Solids and Semiconductor Physics, National Academy of Sciences of Belarus, P. Brovka str. 17, 220072 Minsk, Belarus
[2] Laboratoire CRISMAT, ISMRA, 6 Boulevard du Maréchal Juin 14050 Caen Cedex, France
[3] Institute of Physics, Polish Academy of Sciences, Lotnikov str. 32/46, 02-668 Warsaw, Poland

Received 30 April 2004 / Received in final form 14 July 2004
Published online 26 November 2004 –

Abstract. The crystal structure, magnetization and electrical transport depending on the temperature and magnetic field for the doped stoichiometric $La^{3+}_{1-x}Sr^{2+}_xMn^{3+}_{1-x}Mn^{4+}_xO^{2-}_3$ as well as anion-deficient $La^{3+}_{1-x}Sr^{2+}_xMn^{3+}O^{2-}_{3-x/2}$ ($0 \leq x \leq 0.30$) ortomanganite systems have been experimentally studied. It is established that the stochiometric samples in the region of the $0 \leq x \leq 0.125$ are an O′-orthorhombic perovskites whereas in the $0.175 \leq x \leq 0.30$ – a rhombohedric. For the anion-deficient system the symmetry type of the unit cell is similar to the stoichiometric one. As a doping level increases the samples in the ground state undergo a number of the magnetic transitions. It is assumed that the samples with the large amount of oxygen vacancies are a cluster spin glasses ($0.175 < x \leq 0.30$) and temperature of the magnetic moment freezing is ∼40 K. All the anion-deficient samples are semiconductors and show considerable magnetoresistance over a wide temperature range with a peak for the $x = 0.175$ only. Concentration dependences of the spontaneous magnetization and magnetic ordering temperature for the anion-deficient $La^{3+}_{1-x}Sr^{2+}_xMn^{3+}O^{2-}_{3-x/2}$ system have been established by the magnetic measurements and compared with those for the stoichiometric $La^{3+}_{1-x}Sr^{2+}_xMn^{3+}_{1-x}Mn^{4+}_xO^{2-}_3$ one. The magnetic propeprties of the anion-deficient samples may be interpreted on the base of the superexchange interaction and phase separation (chemical disorder) models.

PACS. 75.30.Kz Magnetic phase boundaries (including magnetic transitions, metamagnetism, etc.) – 75.30.Vn Colossal magnetoresistance – 75.50.Dd Nonmetallic ferromagnetic materials

1 Introduction

The rare-earth doped manganites $Ln^{3+}_{1-x}A^{2+}_xMn^{3+}_{1-x}Mn^{4+}_xO^{2-}_3$ (Ln = La, Pr, Nd; A = Ca, Sr, Ba) have been extensively studied in the last decade owing to their colossal magnetoresistance properties [1–4]. Among the interesting features of the manganites can to distinguish also the metal-insulator transition [5] near the Curie point often accompanied by the charge [6] and orbital [7] ordering. It is now widely accepted that the variety of their physical properties are caused by the strong correlation and (or) competition of the lattice, orbital, charge and spin degrees of freedom.

Undoped stoichiometric $La^{3+}Mn^{3+}O^{2-}_3$ compound has an O′-orthorhombic (space group Pnma, $Z = 4$) crystal structure at the room temperature and shows the orbital ordering due to the strong cooperation static Jahn-Teller interaction [8]. Important feature of the manganites is that a Mn^{3+} ion is a Jahn-Teller one. In the parent material the Mn^{3+} ions have a $3d^4$ configuration where the three electrons occupy all the three t_{2g} degenerated orbitals, while one electron occupies the one from two e_g orbitals. Jahn-Teller distortions are originated when the degeneration of e_g orbitals disappears. The orbital ordering in $LaMnO_3$ consists of the alternate arrangements of d_{z^2} and $d_{x^2-y^2}$ orbitals in (001) planes. The orbital ordering along [001] axis is the antiferrodistortion. The number of the e_g electrons makes the parent $LaMnO_3$ Mott-type antiferromagnetic insulator [9,10].

The substitution of $LaMnO_3$ by divalent ions oxidizes Mn^{3+} to Mn^{4+} and transforms the antiferromagnetic insulating state to the ferromagnetic metallic one [11]. The cooperative static Jahn-Teller distortion strongly depends on concentration of Mn^{3+}. Therefore the influence of the

[a] e-mail: truhanov@ifttp.bas-net.by

Jahn-Teller distortion has to taken into account to understand the magnetic and electrotransport properties of the lightly doped manganites.

Connection between the ferromagnetism and electrical conduction in the doped manganites is often explained in terms of so called double exchange mechanism [12,13]. However, some authors have been pointed out that the double exchange only is inadequate for the explaining many physical properties of the systems in question. There have been proposed the different mechanisms to interpret the nature of interesting features of manganites: the indirect superexchange interaction [14] and phase separation [15,16]. For the lightly doped insulating regime the double exchange model suggested a homogeneous canted antiferromagnetism. However, NMR experiments for quite a few manganites have been interpreted in terms of the phase separation and mixture of magnetic states [17]. Neutron diffraction [18] and HREM results [19] also support this point of view.

The $La_{1-x}Sr_xMnO_3$ solid solutions are the best example of double exchange system. It has the largest one-electron bandwidth and is therefore less affected by Coulomb correlations. However as we have already noted above the lightly doped manganites is strongly influenced by the cooperative static Jahn-Teller distortion. An average manganese valence may be changed by the different methods leading to the modification of the exchange interactions.

It is interesting to investigate the magnetic and electrotransport properties of the doped manganites with monovalent Mn^{3+} manganese ions. Such situation is realized in the anion-deficient doped $La^{3+}_{1-x}Sr^{2+}_xMn^{3+}O^{2-}_{3-x/2}$ manganites. It should be noted that the dependence of the physical properties of the hole-doped perovskite manganites on the oxygen stoichiometry has been weakly investigated until now.

The influence of the oxygen vacancies on the Curie temperature T_C and electrical resistivity ρ for the La – Sr – Mn – O samples have been earlier investigated [20–22]. The decrease of T_C and saturation magnetization M_S as well as the rise of the electrical resistivity with increasing the oxygen deficiency δ is detected. These features have been explained by weakening the ferromagnetic double exchange interactions because of decreasing the ratio Mn^{3+}/Mn^{4+}.

The removal of one oxygen ion from the crystal lattice of the manganites produces a reduction process when two Mn^{4+} ions are converted to two Mn^{3+} ones and their coordination number decreases [23]. This process will weaken the exchange interaction intensity because of the reducing of the double exchange (Mn^{3+} – O – Mn^{4+}) and superexchange (Mn^{3+} – O – Mn^{3+}) mechanisms. In this paper, we describe the experimental results of the crystal structure, magnetic and electrotransport measurements of the anion-deficient $La^{3+}_{1-x}Sr^{2+}_xMn^{3+}O^{2-}_{3-x/2}$ manganites and their comparative analysis with the stoichiometric $La^{3+}_{1-x}Sr^{2+}_xMn^{3+}_{1-x}Mn^{4+}_xO^{2-}_3$ ones. We draw attention that the double exchange mechanism is inapplicable for the interpretation of the magnetic properties of the anion-deficient system.

2 Experiment

Polycrystalline stoichiometric $La_{1-x}Sr_xMnO_3$ ($x = 0.05$; 0.075; 0.10; 0.125; 0.175; 0.225 and 0.30) samples have been fabricated with conventional ceramic technology. La_2O_3 (99.99%), $SrCO_3$ (99.99%) and MnO_2 (99.99%) have been mixed in the designed cation ratios ($La : Sr : Mn = [1 - x] : x : 1$) and ground into an agate mortar with a small value of ethanol. La_2O_3 oxide has been dried at 1000 °C for 2 h before weighing. The obtained mixtures have been pressed into pellets and prefired at 1100 °C for 2 h in air to decompose strontium carbonate to strontium oxide. Obtained pellets have been again ground, compacted and synthesized at 1550 °C during 4 h in air followed by slow cooling at a rate of 95 °Ch^{-1} in order to receive stoichiometric oxygen content.

All the synthesized compounds have been checked by powder X-ray diffraction method to determine the qualitative phase content and unit cell parameters. X-ray data have been recorded at room temperature with a DRON-3 diffractometer in Cr-K_α radiation in angle range of 30 deg $\leq 2\theta \leq$ 100 deg. The oxygen content of all the sintered samples has been determined by the thermogravimetric analysis in a reducing H_2/N_2 flow at 600 °C. These investigations have shown the oxygen content to be stoichiometric. As it is known the deviation of the oxygen stoichiometry for the manganites prepared by aforementioned technique has been negligible [24]. We determined the Mn valence by redox titration. This study gave values of Mn^{4+} concentration equal to 5.3% and 30.1% for the stoichiometric $La_{0.95}Sr_{0.05}MnO_3$ and $La_{0.70}Sr_{0.30}MnO_3$ compounds, respectively. The differences between the content of Mn^{4+} and x appear probably from small oxygen non-stoichiometry or cation impurities.

Polycrystalline anion-deficient $La_{1-x}Sr_xMnO_{3-x/2}$ samples have been received by the topotactic reaction method. The topotactic reaction is one without the considerable changes of the as-prepared crystal structure. Often the topotactic product is metastable. To obtain the oxygen vacancies the samples have been treated in the evacuated soldered with two sides silica tubes at 900 °C during 2 h using metallic tantalum as an oxygen getter. The final oxygen content has been calculated from a change of the sample weight after reduction. Relative error of the oxygen content measurements has not exceeded 0.3%.

To check the oxygen content in the anion-deficient samples they have been subjected to the reoxidation in air at 900 °C during 2 h. The weight gain resulted from the reoxidation has indicated that the oxygen deficit of the anion-deficient samples has been found with an error ±0.01. This fact confirms the topotactic character of the reduction because an important feature of the oxygen deficient perovskite compounds is their ease of reoxidation with the restoration of their initial composition, structure and physical properties.

The magnetization measurements have been made using a OI-3001 commercial vibrating sample magnetometer in the temperature range of 4.2–200 K. The magnetic ordering temperature ($T_{\rm MO}$) has been defined as an point where the field cooled (FC) magnetization value is less than 10% of the total one in field of 100 Oe. The ferromagnetic cluster freezing temperature (T_f) has been determined as an point of the zero field cooled (ZFC) magnetization peak. The value of spontaneous magnetic moment (M_S) has been determined by the field dependence of magnetization by extrapolation to zero field. The alternating current (ac) magnetic susceptibility has been measured with a superconducting quantum interference device (Quantum Design, USA). Ac-susceptibility measurements have been made with the different frequencies F = 100, 1000 and 10000 Hz under ac-field of 10 Oe. The electrical resistivity has been obtained by a standard four-probe method in the temperature range of 78–400 K. Indium eutectic has been employed for ultrasonic deposition of the contacts. For these measurements well-sintered samples in the form of $10 \times 2 \times 2$ mm^3 parallelepiped have been used. The magnetoresistance has been calculated according to the relation:

$$MR(\%) = \{[\rho(H) - \rho(0)]/\rho(0)\} \times 100\% \qquad (1)$$

where $MR(\%)$ – negative isotropic magnetoresistance in percent, $\rho(H)$ – electrical resistivity in magnetic field of 9 kOe, $\rho(0)$ – electrical resistivity without magnetic field. Applied magnetic field has been applied parallel to the current in the sample during the magnetoresistance measurements.

3 Results and discussion

The crystal structure and phase composition for both the stoichiometric $La_{1-x}Sr_xMnO_3$ and anion-deficient $La_{1-x}Sr_xMnO_{3-x/2}$ samples have been checked by powder X-ray diffraction. XRD data are presented in Figure 1. It is established that both the stoichiometric and anion-deficient samples have perovskite structure. In the region of the $0 \le x \le 0.125$ the stochiometric samples are described by the O′-orthorhombic unit cell with Pbnm space group and $Z = 4$ (the number of the formula units into the unit cell), whereas at the $0.175 \le x \le 0.30$ – rhombohedric one with R$\bar{3}$c space group and $Z = 2$. For the anion-deficient samples the symmetry type of the unit cell is similar to stoichiometric one. The parameters of the unit cell for the both systems are collected in Tables 1 and 2.

The O′-orthorhombic → rhombohedric structural transition for the stoichiometric $La_{1-x}Sr_xMnO_3$ single crystals at the $x = 0.175$ has been earlier detected [25]. In the work [26] the O′-orthorhombic structural phase have been revealed for the $La_{1-x}Sr_xMnO_3$ sample with the Mn^{4+} concentration equal to 12%, while for the 27% – rhombohedric one. For the oxygen excess $LaMnO_{3+\delta}$ samples the O′-orthorhombic → rhombohedric structural transition have been observed in the range 12%–18% of the Mn^{4+} concentration [27]. For the anion-deficient

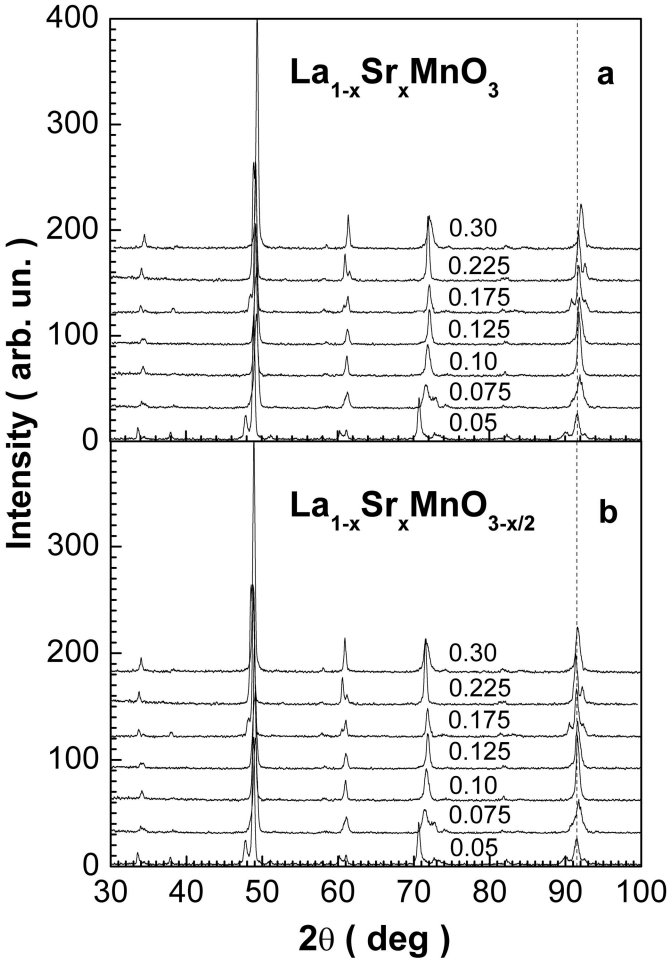

Fig. 1. The room temperature powder X-ray diffraction patterns for the stoichiometric $La_{1-x}Sr_xMnO_3$ (a) and anion-deficient $La_{1-x}Sr_xMnO_{3-x/2}$ (b) samples.

$La_{0.70}Sr_{0.30}MnO_{3-\delta}$ samples [22] X-ray diffraction analysis shows the R → O′ phase transition at the $0.075 \le \delta \le 0.1$ with increase of δ. We have also observed earlier such character of the unit cell symmetry changing for the doped anion-deficient $La_{1-x}Ca(Ba)_xMnO_{3-x/2}$ systems [28,29]. It should be noted the similar X-ray reflexes are shifted to low Brag's angles in the anion-deficient case Figure 2 that corresponds to the larger unit cell volume in comparison with the stoichiometric one. The larger x the stronger this shifting.

The determination of the Jahn-Teller transition temperatures for the non-stoichiometric system is desirable since a such situation may be realized when the anion-deficient samples have T_{JT} above the room temperature for the $x < 0.125$, while for the $x > 0.175$ it is below one. In present manuscript the determination of the T_{JT} is not carried out. As we know T_{JT} for the stoichiometric $La_{0.90}Sr_{0.10}MnO_3$ is 573 K [30]. For the anion-deficient samples T_{JT} may be assumed well below.

O′-orthorhombic ($c/\sqrt{2} < a \le b$) unit cell originates from the cooperative static Jahn-Teller distortion [31]. For the stoichiometric $La_{1-x}Ca_xMnO_3$ system with doping

Table 1. Symmetry (O′-O′-orthorhombic and R-rhombohedric) and parameters (a, b, c, α and V) of the unit cell for the stoichiometric $La_{1-x}Sr_xMnO_3$ ($0 \leq x \leq 0.30$) samples.

Composition	Symmetry	a, Å	b, Å	c, Å	α, deg	V, Å^3
$LaMnO_3$	O′	5.556	5.686	7.731		244.19
$La_{0.95}Sr_{0.05}MnO_3$	O′	5.528	5.641	7.737		241.19
$La_{0.925}Sr_{0.075}MnO_3$	O′	5.526	5.618	7.743		240.38
$La_{0.90}Sr_{0.10}MnO_3$	O′	5.523	5.594	7.746		239.31
$La_{0.875}Sr_{0.125}MnO_3$	O′	5.521	5.574	7.751		238.54
$La_{0.825}Sr_{0.175}MnO_3$	R	5.489			60.60	237.32
$La_{0.775}Sr_{0.225}MnO_3$	R	5.480			60.52	235.52
$La_{0.70}Sr_{0.30}MnO_3$	R	5.464			60.44	233.64

Table 2. Symmetry (O′-O′-orthorhombic and R - rhombohedric) and parameters (a, b, c, α and V) of the unit cell for the anion-deficient $La_{1-x}Sr_xMnO_{3-x/2}$ ($0 \leq x \leq 0.30$) samples.

Composition	Symmetry	a, Å	b, Å	c, Å	α, deg	V, Å^3
$LaMnO_3$	O′	5.556	5.686	7.731		244.19
$La_{0.95}Sr_{0.05}MnO_{2.98}$	O′	5.551	5.642	7.748		242.67
$La_{0.925}Sr_{0.075}MnO_{2.96}$	O′	5.547	5.620	7.753		241.68
$La_{0.90}Sr_{0.10}MnO_{2.95}$	O′	5.544	5.588	7.767		240.61
$La_{0.875}Sr_{0.125}MnO_{2.94}$	O′	5.540	5.575	7.770		239.97
$La_{0.825}Sr_{0.175}MnO_{2.91}$	R	5.523			60.08	238.25
$La_{0.775}Sr_{0.225}MnO_{2.89}$	R	5.513			60.06	236.96
$La_{0.70}Sr_{0.30}MnO_{2.85}$	R	5.507			60.04	236.19

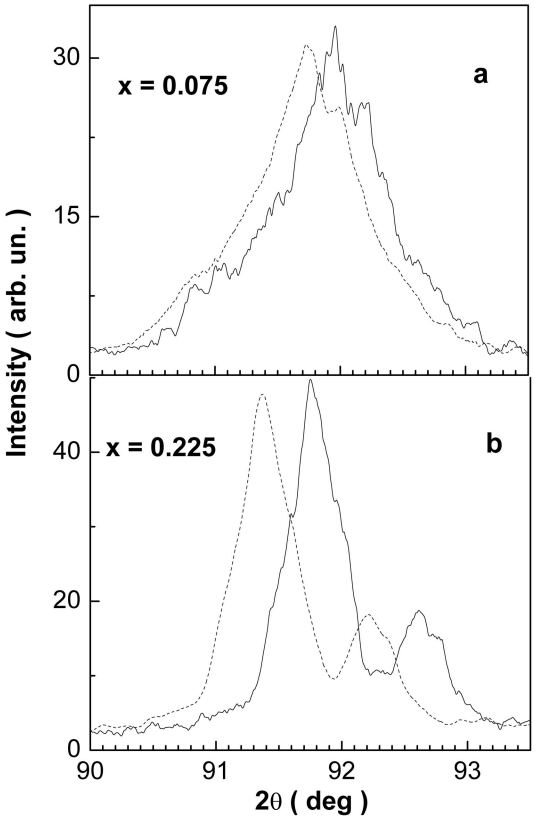

Fig. 2. The (132+024+312+204) and ($42\bar{2}$ + 422 + $\bar{4}22$) X-ray reflexes for the $x = 0.075$ (a) and 0.225 (b) samples, respectively. Solid line denotes data for the stoichiometric $La_{1-x}Sr_xMnO_3$ samples, dash – for the anion-deficient $La_{1-x}Sr_xMnO_{3-x/2}$ ones.

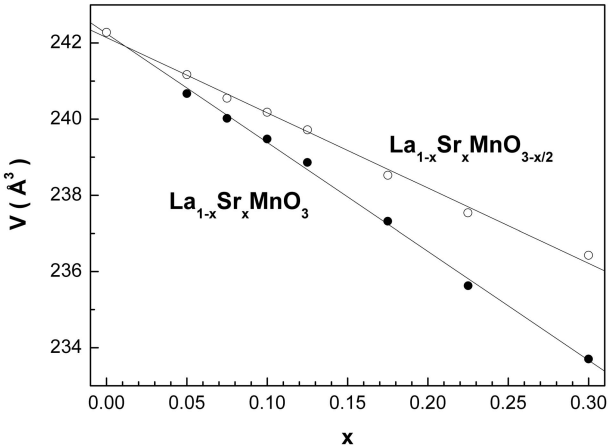

Fig. 3. The concentration dependence of the comparable unit cell volume for the stoichiometric $La_{1-x}Sr_xMnO_3$ (full circle) and anion-deficient $La_{1-x}Sr_xMnO_{3-x/2}$ (open circle) samples.

the crystal structure transition from the O′-orthorhombic to O-orthorhombic ($a < c/\sqrt{2} < b$) symmetry occurs at $x \sim 0.1$ [28]. In our case transition from the O′-orthorhombic to rhombohedric unit cell is fixed at $x = 0.175$. It is reasonable to propose that O′ → R transition may be produced by domination of dimensional effect over the Jahn-Teller one. In the case of anion-deficient Ba-doped system similar situation is realized [29]. It is well known that in the 12-coordination the effective ionic radii for the Sr^{2+} (1.44 Å) and Ba^{2+} (1.61 Å) are larger those than for the La^{3+} (1.36 Å) and Ca^{2+} (1.34 Å) [32].

With doping the unit cell volume decreases monotonically for both the $La_{1-x}Sr_xMnO_3$ and $La_{1-x}Sr_xMnO_{3-x/2}$ systems (Fig. 3). For the stoichiometric samples this may be explained by the

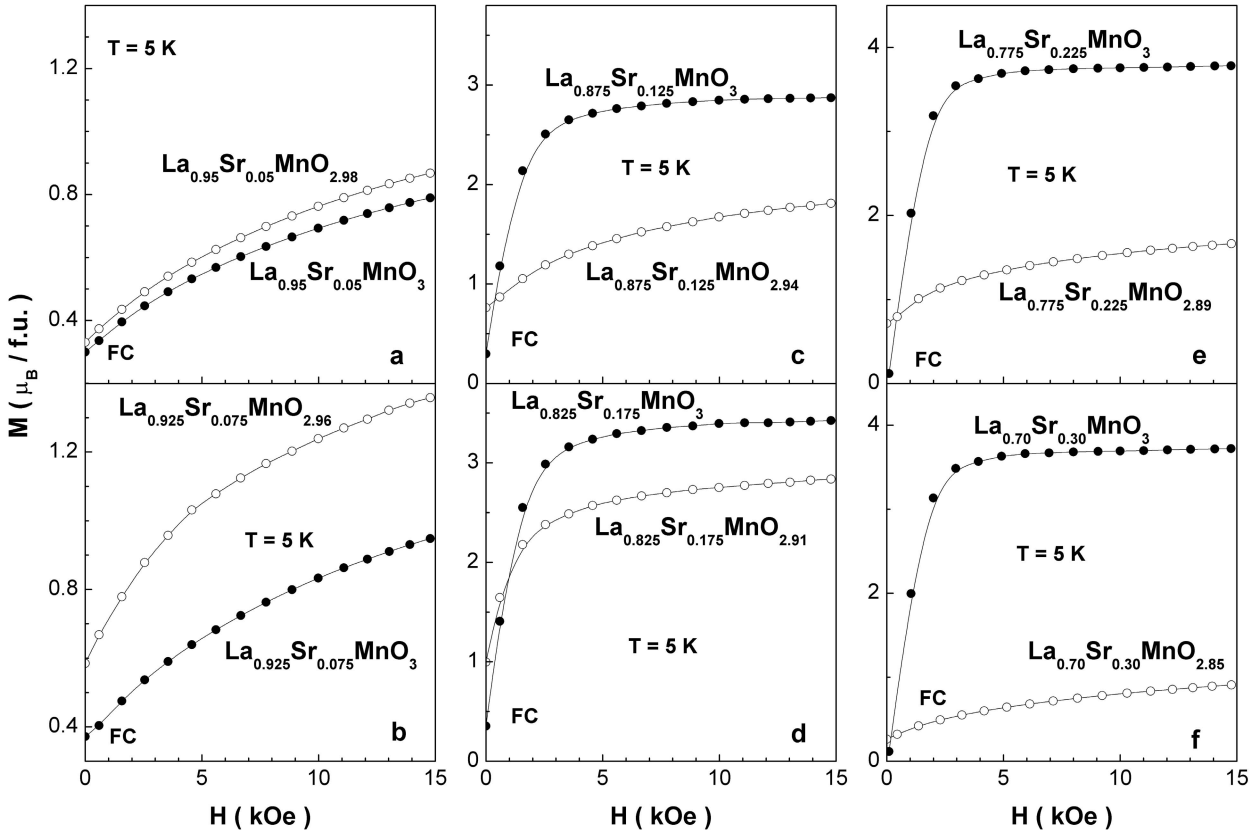

Fig. 4. The FC magnetization vs. field at the 5 K for the stoichiometric $La_{1-x}Sr_xMnO_3$ (full circle) and anion-deficient $La_{1-x}Sr_xMnO_{3-x/2}$ (open circle) samples with $x = 0.05$ (a), 0.075 (b), 0.125 (c), 0.175 (d), 0.225 (e) and 0.30 (f).

conversion of the Mn^{3+} into Mn^{4+} ions. It is known that $r[Mn^{3+}] = 0.645$ Å larger than $r[Mn^{4+}] = 0.530$ Å for octahedral coordination [32]. Therefore the increase of A-sublattice is compensated by the decrease of B-sublattice and the unit cell volume decreases. In the anion-deficient $La^{3+}_{1-x}Sr^{2+}_x Mn^{3+}O^{2-}_{3-x/2}$ case the samples have only Mn^{3+} ions. However their coordination number along with the effective ionic radius decreases as x rises. $r[Mn^{3+}] = 0.580$ Å for the pentahedral anion surrounding [32]. The presence of the real oxygen vacancies leads to decreasing of unit cell volume. It should be noted that this process is less expressed for the anion-deficient $La^{3+}_{1-x}Sr^{2+}_x Mn^{3+}O^{2-}_{3-x/2}$ system.

$La_{0.925}Sr_{0.075}MnO_3$ demonstrates transition to the paramagnetic state at $T_N \approx 144$ K which is some larger than one for the parent $LaMnO_3$. For the significant doping levels T_C constantly increases with x. So in region of the $0.125 \leq x \leq 0.30$ Curie temperature increases from 190 to 350 K. All the ac-susceptibility curves are followed by the Curie-Weis law. Such behavior of the magnetic properties well agrees with the earlier obtained results [25].

The field dependences of magnetization at $T = 5$ K for both the stoichiometric $La_{1-x}Sr_xMnO_3$ and anion-deficient $La_{1-x}Sr_xMnO_{3-x/2}$ systems are displayed in Figure 4. In fields up to 15 kOe magnetization for the some stoichiometric ($x = 0.05$ and 0.075) and all the anion-deficient samples is not saturated. Therefore it is difficult to estimate the spontaneous magnetization per Mn ion. For the stoichiometric system magnetization always rises with increase x. For the $La_{0.775}Sr_{0.225}MnO_3$ and $La_{0.70}Sr_{0.30}MnO_3$ samples only spontaneous magnetization achieves the theoretically possible values 3.78 and 3.70 μ_B per Mn ion, respectively. Magnetization of all the anion-deficient samples at first increases up to $x = 0.175$ and then decreases. It should be noted that magnetization for the almost all (except $x = 0.05$ and 0.075) $La_{1-x}Sr_xMnO_{3-x/2}$ is well less than one for the $La_{1-x}Sr_xMnO_3$.

The temperature dependences of ZFC and FC magnetizations for the some anion-deficient $La_{1-x}Sr_xMnO_{3-x/2}$ samples are showed in Figure 5. The samples with $x = 0.05$ and 0.075 demonstrate an gradual increase of FC magnetization below 120 and 105 K, respectively. It is worth nothing that these temperatures are enough less than $T_N \approx 140$ K for $LaMnO_3$ [9]. For the $La_{0.95}Sr_{0.05}MnO_{2.98}$ sample the temperature of the ZFC magnetization peak coincides with $T_{MO} \approx 120$ K, while for the $La_{0.925}Sr_{0.075}MnO_{2.96}$ the ZFC curve starts to differ significantly from the FC one just below T_{MO}. At this point ($T_f \approx 91$ K) it has a small peak and does not depend on temperature in practice. The $La_{0.90}Sr_{0.10}MnO_{2.95}$ sample has lowest $T_{MO} \approx 101$ K. The transition to the

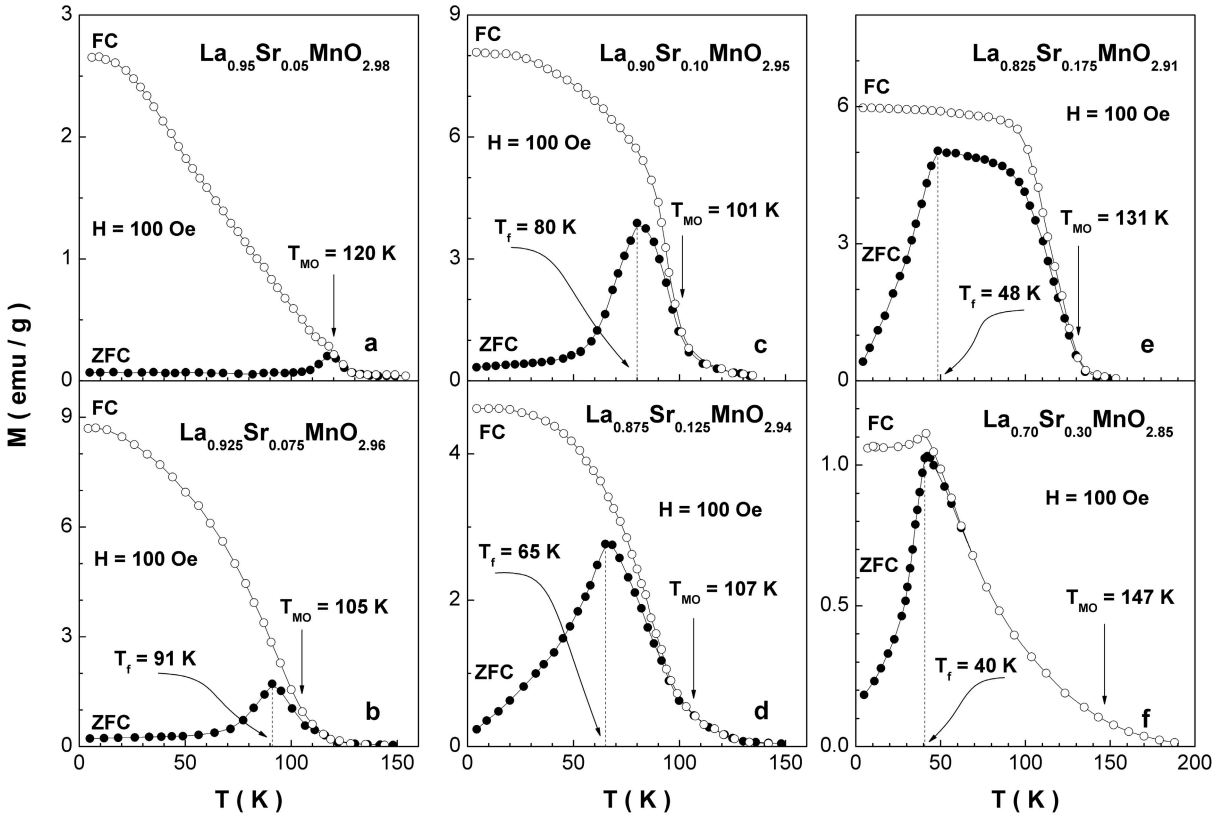

Fig. 5. The ZFC (full circle) and FC (open circle) magnetizations vs. temperature in the magnetic field of the 100 Oe for the anion-deficient $La_{1-x}Sr_xMnO_{3-x/2}$ samples with $x = 0.05$ (a), 0.075 (b), 0.10 (c), 0.125 (d), 0.175 (e) and 0.30 (f).

paramagnetic state in the region of the $0.10 \leq x \leq 0.175$ is well defined, which is characteristic of homogeneous magnetic state. The $La_{0.825}Sr_{0.175}MnO_{2.89}$ sample has $T_{MO} \approx$ 131 K and is one from all the other which has a biggest liner part of ZFC magnetization. ZFC peak in this case is fixed at $T_f \approx 48$ K. In the region of the $0.175 < x \leq 0.30$ difficult to determine the magnetic ordering temperature because the transition to paramagnetic state is very broad. This may be characteristic of an inhomogeneous initial magnetic state. The samples in this region are most probable cluster spin glasses. Such scenario is confirmed by the pronounced peak at $T_f \approx 45$ K. It should be noted that T_f continuously decreases, whereas x increases which corresponds to reduction of the ferromagnetic cluster size [33].

In Figure 6 the ac-magnetic susceptibility for the anion-deficient $La_{0.70}Sr_{0.30}MnO_{2.85}$ sample is shown. The initial susceptibility have been measured at the different frequencies as a function of temperature. The curves display a maximum at the temperature which shifts upwards with increasing frequency. This is a distinct feature of a spin glass state. The peak which is seen in the initial susceptibility at the lowest frequency measured (100 Hz) has been taken as the spin glass freezing temperature T_f. This peak temperature coincides well with one seen in the ZFC magnetization (Fig. 5f). At this temperature the irreversibility between FC and ZFC magnetization is very strong.

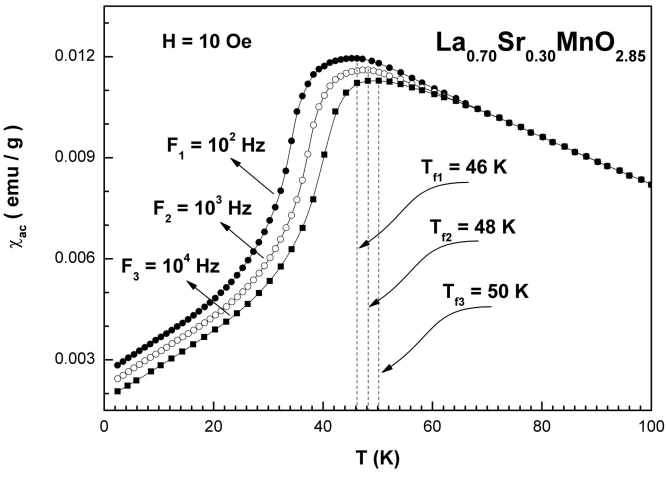

Fig. 6. Frequency dispersion ($F = 100$, 1000 and 10 000 Hz) of the initial ac-magnetic susceptibility in the field of 10 Oe for the anion-deficient $La_{0.70}Sr_{0.30}MnO_{2.85}$ sample.

The electrical resistivity as function of a temperature for the some stoichiometric $La_{1-x}Sr_xMnO_3$ and anion-deficient $La_{1-x}Sr_xMnO_{3-x/2}$ samples are displayed in Figure 7. All the reduced samples have a resistivity of the semiconductor type. In contrast to the stoichiometric $La_{1-x}Sr_xMnO_3$ system there is no metal-insulator transition even for the anion-deficient $x = 0.175$ sample showing the largest ferromagnetic component. The resistivity

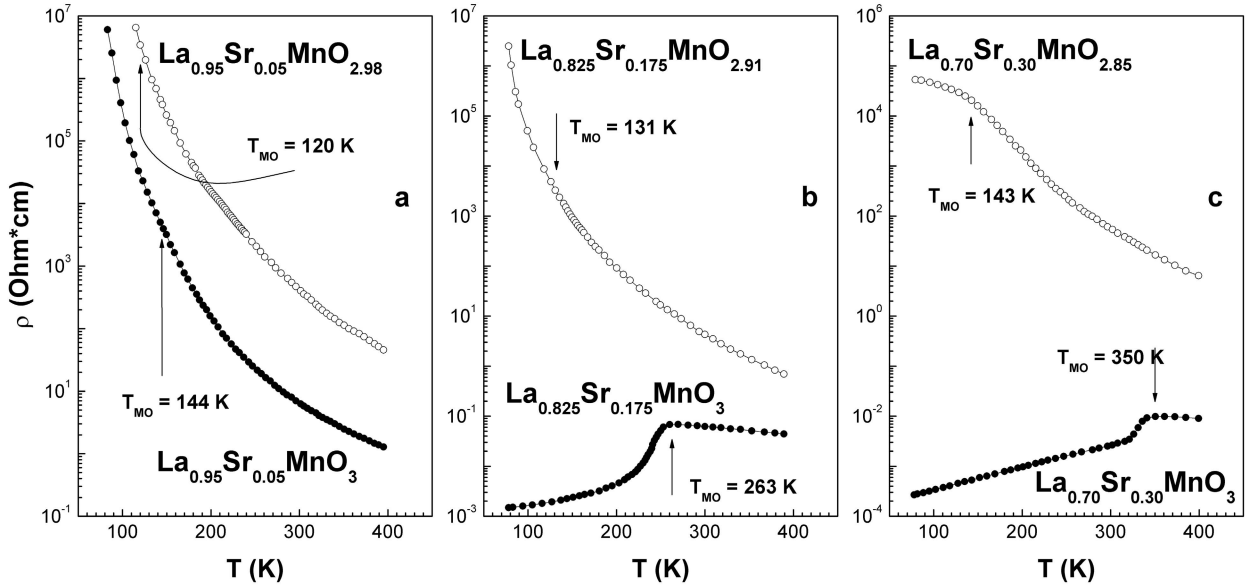

Fig. 7. The electrical resistivity vs. temperature for the stoichiometric $La_{1-x}Sr_xMnO_3$ (full circle) and anion-deficient $La_{1-x}Sr_xMnO_{3-x/2}$ (open circle) samples with $x = 0.05$ (a), 0.175 (b) and 0.30 (c).

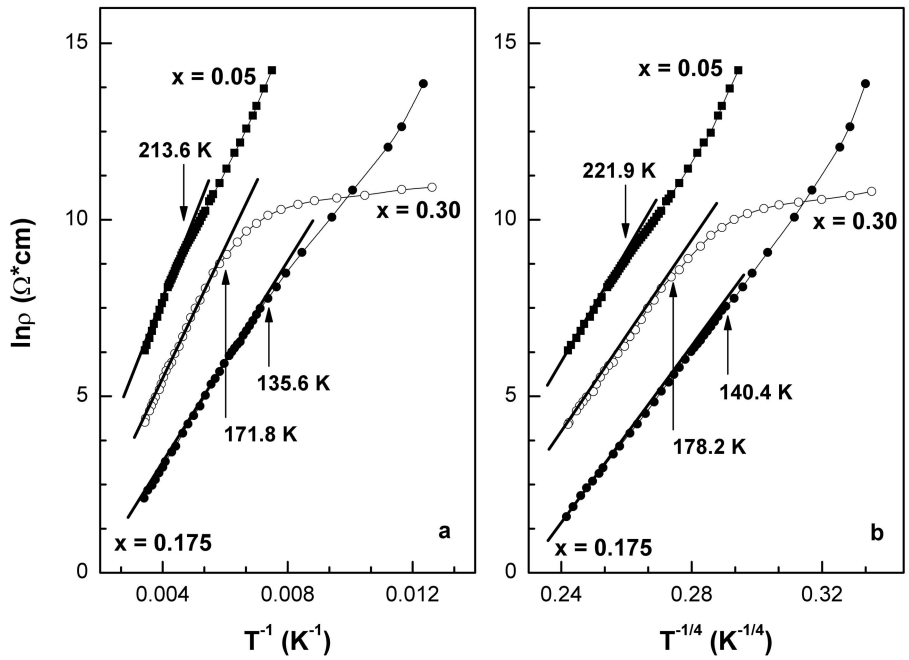

Fig. 8. Fitting of the electrical resistivity to T^{-1} (a) and $T^{-1/4}$ (b) for the anion-deficient $La_{1-x}Sr_xMnO_{3-x/2}$ samples with $x = 0.05$ (full rectangle), 0.175 (full circle) and 0.30 (open circle).

for the anio-deficient samples always increases as temperature decreases. At the room temperature resistivity of the anion-deficient samples gradually decreases as doping level increases and at the $x = 0.175$ it starts to rise up to $x = 0.30$.

We attempt to analyse the resistivity data. Thermal activation model:

$$\rho = \rho_0 \exp\{E_{AC}/k_B T\} \tag{2}$$

and Mott's variable range hoping one:

$$\rho = \rho_0 \{T_0/T\}^{1/4} \tag{3}$$

have been chosen to fit ρ-T curves. In Figure 8 the $\ln\rho \sim T^{-1}$ and $\ln\rho \sim T^{-1/4}$ relations are given. It is interesting that the $\ln\rho$ curves at the high temperatures (in paramagnetic regime) are better fitted by the thermal activation model. Such situation allows to calculate the activation energy. The angle of the tangent to the $\ln\rho \sim T^{-1}$ curve

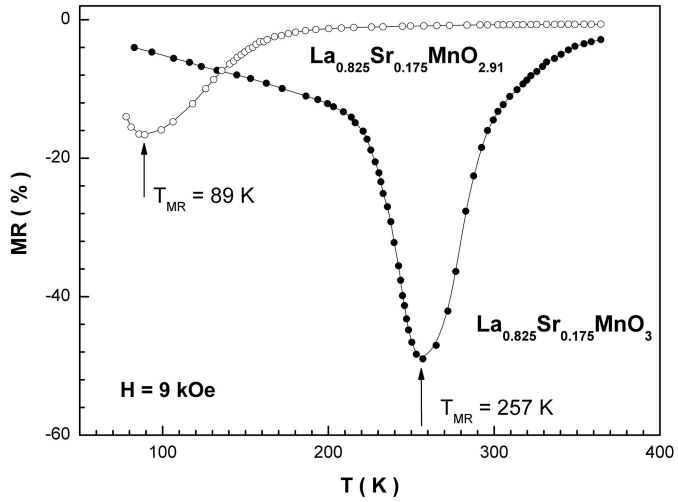

Fig. 9. The magnetoresistance vs. temperature in the field of 9 KOe for the stoichiometric $La_{0.825}Sr_{0.175}MnO_3$ (full circle) and anion-deficient $La_{0.825}Sr_{0.175}MnO_{2.91}$ (open circle) samples.

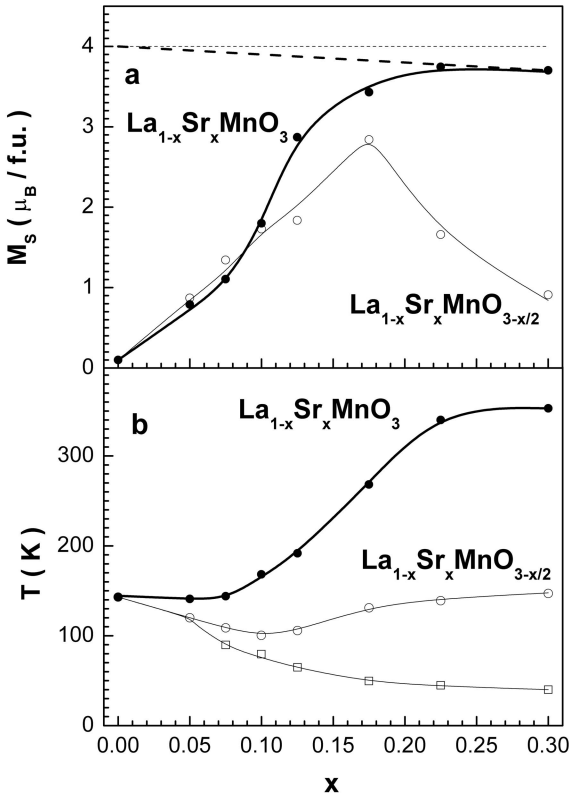

Fig. 10. The concentration dependence of the magnetization in the field of 15 kOe at the 5 K for the stoichiometric $La_{1-x}Sr_xMnO_3$ (full circle) and anion-deficient $La_{1-x}Sr_xMnO_{3-x/2}$ (open circle) samples (a). Solid lines construct on basis of the experimentally observed values for the stoichiometric (thick line) and anion-deficient (thin line) samples. Dash lines denote the theoretically calculated values of the saturation magnetization for the stoichiometric (thick line) and anion-deficient (thin line) samples. The concentration dependence of the magnetic transition temperatures (b) for the stoichiometric $La_{1-x}Sr_xMnO_3$ (full circle) and anion-deficient $La_{1-x}Sr_xMnO_{3-x/2}$ (open symbol) samples. Open circle denotes the magnetic ordering temperature, open rectangle – the freezing temperature.

is proportional the activation energy. At the low temperatures the activation energy decreases. Transport above T_C is still a matter of controversy as numerous groups have reported different behaviour. The simple activation law could indicate the opening of a gap at the Fermi level above T_C. Photoemission data support the view that a small bandgap appears at T_C in the $La_{0.7}Sr_{0.3}MnO_3$ [34].

All the $La_{1-x}Sr_xMnO_{3-x/2}$ samples show a magnetoresistance enough below a point where spontaneous magnetization develops. There is peak of magnetoresistance about 18% for the $x = 0.175$ only at the $T_{MR} \approx 89$ K (Fig. 9). For the stoichiometric sample the magnetoresistance peak is observed at the 257 K that is slightly below the T_{MO}. For all the anion-deficient samples the gradual magnetoresistance increase up to the liquid nitrogen temperature has been observed, which is typical for conducting magnetic ceramics. The maximum $MR = 22\%$ has been observed for the $x = 0.30$. This type of magnetoresistance is possible due to an intergranular electrical transport.

Summarizing our magnetization and electrical data, we construct the concentration dependence of the magnetization in field of 15 kOe at $T = 5$ K and magnetic transition temperatures (Fig. 10) for both the stoichiometric $La_{1-x}Sr_xMnO_3$ and anion-deficient $La_{1-x}Sr_xMnO_{3-x/2}$ samples. The saturation magnetization values for both systems calculated in accordance with relation:

$$\sigma = Ng\mu_B S_{ave} \tag{4}$$

where N is a number of Mn ions per unit volume, g – the gyromagnetic ratio (∼2), μ_B – the Bohr magneton and S_{ave} – the average spin equal $[1 - x]\{S(Mn^{3+}) = 2\} + x\{S(Mn^{4+}) = 3/2\}$. For the anion-deficient system $S_{ave} \approx 2$ $\{S(Mn^{3+}) = 2\}$. The calculations have been realized assuming that all the $3d$ electrons of Mn ions contribute with their spins only and all exchange manganese interactions are ferromagnetic [35]. The magnetization achieves the theoretically calculated value only for the $La_{0.775}Sr_{0.225}MnO_3$ and $La_{0.70}Sr_{0.30}MnO_3$ samples. Such behavior of magnetization well agrees with earlier obtained results by other authors [11,25,36]. It is shown that the M_S for the anion-deficient system enough well coincides with M_S for the stoichiometric one in the range $0 \leq x \leq 0.075$ although it is much less than the theoretical value. For the anion-deficient samples increasing Sr content up to $x = 0.175$ leads to an increase (approximately linear) of the magnetization from ∼0.1 ($x = 0$) to ∼2.84 μ_B/f. u. (∼70% of expected value for the truly ferromagnetic ordering of $x = 0.175$), and then it drops down to ∼0.90 μ_B/f. u. ($x = 0.30$).

The concentration dependence of the magnetic transition temperatures for both the stoichiometric $La_{1-x}Sr_xMnO_3$ and anion-deficient $La_{1-x}Sr_xMnO_{3-x/2}$ samples is constructed in Figure 10. It is well known

that the $LaMnO_3$ is an orbital ordered antiferromagnet of A-type with $T_N \approx 140$ K. A weak ferromagnetic component is due to an antisymmetric exchange Dzyaloshinsky-Moriya's interaction [37,38]. As x rises from 0 to 0.10 T_{MO} decreases from 140 to 101 K. In this region the $La_{1-x}Sr_xMnO_{3-x/2}$ samples are most likely mixture of orbital ordered antiferromagnetic phase and ferromagnetic clusters. In the region of the $0.10 \leq x \leq 0.175$ the ground state appears be mixture consisting from ferromagnetic and orbital disordered antiferromagnetic phases. $La_{0.825}Sr_{0.175}MnO_{2.89}$ sample has $T_C \approx 131$ K. The ferromagnet-paramagnet transition is realized through inhomogeneous magnetic state with the ferromagnetic correlations above T_f. For the $x > 0.175$ the anion-deficient samples are most likely cluster spin glasses with $T_f \approx$ 40 K. It should be noted that such temperature is typical for the spin glass state in manganites [33,39]. The information about magnetic phase states for the stoichiometric $La_{1-x}Sr_xMnO_3$ samples may be obtained elsewhere [40–42].

The anion-deficient $La_{1-x}Sr_xMnO_{3-x/2}$ samples are interesting for study indirect superexchange interactions between Mn ions. It should be noted that La^{3+}, Sr^{2+} and O^{2-} ions are diamagnetic which is facilitated the interpretation of experimental results. In order to explain a behavior of doped manganite systems, Zener elaborated a special theory of indirect exchange interactions via charge carriers. This form of interactions has been given the name of double exchange [12,13]. The double exchange is based on the real transition of an electron from a half-filled e_g orbital of an Mn^{3+} ion to a free e_g orbital of Mn^{4+}. Such a jump is energetically advantageous in the case of parallel arrangement of local spins S of Mn^{3+} and Mn^{4+} ions being nearest neighbors.

Goodenough [43] has suggested that ferromagnetism is not governed by double exchange alone but also by a specific nature of the superexchange interactions in the Mn^{3+} – O – Mn^{3+} Jahn-Teller ion systems. He has supposed that in the case of removing cooperative static Jahn-Teller distortion the orbital configuration of the 3d electrons is determined by the position of the ion nuclei (Goodenough's quasistatic hypothesis). In this case the ferromagnetic fraction of the exchange is determined by a virtual electron transfer from the half-filled eg orbitals of the Mn^{3+} ions to the empty ones. Note that, in accordance with the superexchange, the state of ferromagnetic order may not correlate with the behavior of electrical conductivity.

The double exchange mechanism is inapplicable for the interpretation of the magnetic properties of the anion-deficient $La^{3+}_{1-x}Sr^{2+}_xMn^{3+}O^{2-}_{3-x/2}$ system since it does not contain the Mn^{4+} ions. The superexchange Mn^{3+} – O – Mn^{3+} interactions are anisotropic in the orbital ordered phase (positive in (001) planes and negative in [001] directions) but isotropic in the orbital disordered one (positive in all directions) [44]. Taking this into account we believe the ground state in the range $0 < x \leq 0.10$ appears to be orbital ordered antiferromagnetic similar to $LaMnO_3$ with ferromagnetic clusters. The oxygen vacancy concentration is not enough to remove the orbital ordering so the anisotropic character of superexchange interactions does not change.

In the region of the $0.10 < x \leq 0.175$ ferromagnetic component as well as T_{MO} increases. The anion-deficient sample with $x = 0.175$ is most likely critical value at which cooperative static Jahn-Teller distortion is removed completely but fully ferromagnetic state does not realize since a sign of Mn^{3+} – O – Mn^{3+} superexchange interaction changes. If the orbital ordering is removed the Mn^{3+} – O – Mn^{3+} superexchange interactions are positive. This is the case for the octahedral oxygen coordination of Mn^{3+}. However, these interactions became antiferromagnetic in the five-fold or four-fold coordination [45].

For the anion-deficient samples with $x > 0.175$ the antiferromagnetic orbital disordered part of the superexchange Mn^{3+} – O – Mn^{3+} interactions is enhanced. The antiferromagnetic and ferromagnetic phase volumes apparently become comparable. The competition between ferromagnetic and antiferromagnetic clusters may leads to the cluster spin glass state. The spin freezing behaviour is often observed in the inhomogeneous magnetic systems such as granular films of Co-Cu [46] and Co-Ag [47], where ferromagnetic grains are embedded in a non-ferromagnetic background. For $Eu_xSr_{1-x}S$, the firstneighbour Eu-Eu superexchange interactions are positive, whereas the second-neighbour Eu-Eu ones are negative [48]. The magnetic state of these systems is explained by the competition between the positive and negative exchange interactions. The competing interactions result in frustration of the clusters which leads to a freezing of the magnetic moment of the clusters along a local easy direction below T_f.

A simple explanation can be present for the electrical data. The resistivity of the polycrystalline samples is determined by two contributions, i.e. contribution from the intragrain regions (grains) and contribution from the intergrain regions (grain boundaries). Spin-polarized intergrain tunneling in these compounds has been carefully studied and is known to depend on the grain size and the properties of intergranular matter, which constructs the intergrain barrier [49]. Conductive electrons can hop from grain to grain through spin-dependent tunneling. The probability of an electron tunneling across the intergranular barrier arises, when the magnetic moments of the neighboring grains are not parallel and the electron spin is conserved in tunneling. Randomly oriented moments of grains can be aligned by an external field. This causes a significant increase in the tunnel conductance, thereby reducing resistivity of the granular system. With grain growth, the intergranular tunneling gradually disappears, while the intragranular one is enhanced [50].

Polycrystalline manganites usually show MR effect in two distinct regions. One is pronounced near the magnetic ordering temperature (intragrain MR), the other one is dominant at low temperature where the magnetization is substantial (intergrain MR) [51]. The physical origin of the high-temperature MR has been explained by the existence of magnetic polarons near T_C [52].

Above T_{MO} the anion-deficient samples are paramagnetic insulators and resistivity increases as the temperature decreases. Below T_{MO} an appearance of a metallic state is not observed. The conductivity mechanism of doped manganites is conditioned by 3*d*-Mn and 2*p*-O electronic bands. The doping in $La_{1-x}Sr_xMnO_3$ leads to a decrease in the gap between the 3*d*-Mn and 2*p*-O electronic bands. For the stoichiometric samples above the $x = 0.15$ a pure ferromagnetic state is realized. At concentrations $x > 0.15$ these samples exhibit metal-insulator transition below T_{MO}. This electrotransport behaviour is explained by overlapping of the 3*d*-Mn and 2*p*-O bands. The appearance of oxygen vacancies leads to an extending of the crystal lattice and, therefore, to a splitting of the abovementioned electronic bands. An increase in the concentration of oxygen vacancies give rise to an increase in the gap between 3*d*-Mn and 2*p*-O bands. For the anion-deficient $La_{1-x}Sr_xMnO_{3-x/2}$ samples the doping level $x = 0.175$ is the critical one above which the metallic state is not realized, although the ferromagnetic component is significant. It should also be taken into account that the reduction creates oxygen vacancies at the grain boundaries because diffusion coefficients for oxygen on a grain boundary are larger by one order of magnitude than those in the bulk. The oxygen-poor microdomains appear on the grain surface. As a result the electron transfer between grains is difficult and the resistivity rises. The extraction of oxygen from the grain boundaries leads also to a broadening of the insulating barriers associated with intergrain boundaries so the electrical resistivity should increase too [4].

4 Conclusions

The crystal structure, magnetization and electrotransport properties vs. temperature and magnetic field for both the stoichiometric $La^{3+}_{1-x}Sr^{2+}_xMn^{3+}_{1-x}Mn^{4+}_xO^{2-}_3$ and anion-deficient $La^{3+}_{1-x}Sr^{2+}_xMn^{3+}O^{2-}_{3-x/2}$ ($0 \leq x \leq 0.30$) systems of ortomanganites have been studied. The stochiometric samples in the region of the $0 \leq x \leq 0.125$ are O′-orthorhombic perovskites whereas in the $0.175 \leq x \leq 0.30$ – rhombohedric. For the anion-deficient system the symmetry type of unit cell is similar to stoichiometric one. As doping level increases the anion-deficient samples in ground state likly undergo a transition from antiferromagnet A-type ($x = 0$) through inhomogeneous ferromagnetic and antiferromagnetic ($0 < x \leq 0.175$) state to cluster spin glass ($0.175 < x \leq 0.30$) one. All the anion-deficient samples are semiconductors and show considerable magnetoresistance over a wide temperature range with peak for $x = 0.175$ only. Concentration dependences of spontaneous magnetization and magnetic ordering temperature for the anion-deficient $La^{3+}_{1-x}Sr^{2+}_xMn^{3+}O^{2-}_{3-x/2}$ system of ortomanganites have been established by magnetic measurements and compared with those for the stoichiometric $La^{3+}_{1-x}Sr^{2+}_xMn^{3+}_{1-x}Mn^{4+}_xO^{2-}_3$ one. Magnetic propeprties of the anion-deficient samples may be interpreted on the base of the superexchange interaction and phase separation (chemical disorder) models.

The work was partly supported by Belarus Fund for Basic Research (Project F04R-076), Russian Fund for Basic Research (04-02-81051 RFBR-Bel2004_a) and GPOFI "Nanomaterials and nanotechnologies" (Task 3.3).

References

1. R. Von Helmolt, J. Wecker, B. Holzepfel, L. Sehultz, K. Samwer, Phys. Rev. Lett. **71**, 2331 (1993)
2. K. Chahara, T. Ohno, M. Kasai, Y. Kozono, Appl. Phys. Lett. **63**, 1990 (1993)
3. P. Schiffer, A.P. Ramirez, W. Bao, S.-W. Cheong, Phys. Rev. Lett. **75**, 3336 (1995)
4. S.V. Trukhanov, L.S. Lobanovski, M.V. Bushinsky, I.O. Troyanchuk, H. Szymczak, J. Phys.: Condens. Matter **15**, 1783 (2003)
5. J.W. Lynn, R.W. Erwin, J.A. Borchers, Q. Huang, A. Santoro, Phys. Rev. Lett. **76**, 4046 (1996)
6. Y. Moritomo, H. Kuwahara, Y. Tomioka, Y. Tokura, Phys. Rev. B **55**, 7549 (1997)
7. Y. Tokura, Y. Tomioka, J. Magn. Magn. Mater. **200**, 1 (1999)
8. J.M.D. Coey, M. Viret, S. Von Molnar, Adv. Phys. **48**, 167 (1999)
9. G. Matsumoto, J. Phys. Soc. Jpn **29**, 606 (1970)
10. G. Matsumoto, J. Phys. Soc. Jpn **29**, 615 (1970)
11. G.H. Jonker, J.H. van Santen, Physica (Utrecht) **16**, 337 (1950)
12. C. Zener, Phys. Rev. **82**, 403 (1951)
13. P.G. de Gennes, Phys. Rev. **118**, 141 (1960)
14. J.B. Goodenough, *Magnetism and the Chemical Bond* (Wiley, New-York, 1963)
15. E. Dagotto, T. Hotta, A. Moreo, Phys. Rep. **344**, 1 (2001)
16. E.L. Nagaev, Phys. Repts. **346**, 387 (2001)
17. G. Allodi, R. De Renzi, G. Guidi, F. Licci, M.W. Pieper, Phys. Rev. B **56**, 6036 (1997)
18. E.O. Wollan, W.C. Koehler, Phys. Rev. **100**, 545 (1955)
19. A. Moreo, S. Yunoki, E. Dagotto, Science **283**, 2034 (1999)
20. A.M. De Leon-Guevara, P. Berthet, J. Berthon, F. Millot, A. Revcolevschi, A. Anane, C. Dupas, K. Le Dang, J.P. Renard, P. Veillet, Phys. Rev. B **56**, 6031 (1997)
21. A.M. De Leon-Guevara, P. Berthet, J. Berthon, F. Millot, A. Revcolevschi, J. Alloys Comp. **262**, 163 (1997)
22. N. Abdelmoula, K. Guidara, A. Cheikh-Rouhou, E. Dhahri, J.C. Joubert, J. Solid State Chem. **151**, 139 (2000)
23. B.C. Tofield, W.R. Scott, J. Solid State Chem. **100**, 183 (1974)
24. S.V. Trukhanov, I.O. Troyanchuk, N.V. Pushkarev, H. Szymczak, Sov. Phys. – JETP **95**, 308 (2002)
25. A. Urushibara, Y. Moritomo, T. Arima, A. Asamitsu, G. Kido, Y. Tokura, Phys. Rev. B **51**, 14103 (1995)
26. R. Mahesh, R. Mahendiran, A.K. Raychaudhuri, C.N.R. Rao, J. Solid State Chem. **114**, 297 (1995)
27. J. Topfer, J.B. Goodenough, J. Solid State Chem. **130**, 117 (1997)
28. I.O. Troyanchuk, S.V. Trukhanov, H. Szymczak, J. Przewoznik, K. Bärner, Sov. Phys. – JETP **93**, 161 (2001)
29. S.V. Trukhanov, I.O. Troyanchuk, N.V. Pushkarev, H. Szymczak, Sov. Phys. – JETP **96**, 110 (2003)
30. T. Chatterji, B. Ouladdiaf, P. Mandal, B. Bandyopadhyay, B. Ghosh, Phys. Rev. B **66**, 054403 (2002)
31. J.B. Goodenough, Phys. Rev. **100**, 564 (1955)

32. R.D. Shannon, Acta Crystallogr. A **32**, 751 (1976)
33. J. Blasco, J. Garcia, J.M. de Teresa, M.R. Ibarra, P.A. Algarabel, C. Marquina, J. Phys.: Condens. Matter **8**, 7427 (1996)
34. J.H. Park, E. Vescovo, H.J. Kim, C. Kwon, R. Ramesh, T. Venkatesan, Nature **392**, 794 (1998)
35. S.V. Trukhanov, J. Mater. Chem. **13**, 347 (2003)
36. M. Paraskevopoulos, J. Hemberger, A. Loidi, A.A. Mukhin, V.Yu. Ivanov, A.M. Balbashov, J. Phys.: Condens. Matter **12**, 3993 (2000)
37. I. Dzialoshinsky, J. Phys. Chem. Solids **4**, 241 (1958)
38. T. Moriya, Phys. Rev. **120**, 91 (1960)
39. J.C. Nie, J.H. Wang, B.R. Zhao, J. Magn. Magn. Mater. **192**, L379 (1999)
40. H. Kawano, R. Kajimoto, M. Kubota, H. Yoshizawa, Phys. Rev. B **53**, R14709 (1996)
41. J.S. Zhou, J.B. Goodenough, A. Asamitsu, Y. Tokura, Phys. Rev. Lett. **79**, 3234 (1997)
42. G.L. Liu, J.S. Zhou, J.B. Goodenough, Phys. Rev. B **64**, 144414 (2001)
43. J.B. Goodenough, A. Wold, R.J. Arnott, N. Menyuk, Phys. Rev. **124**, 373 (1961)
44. S.V. Trukhanov, I.O. Troyanchuk, M. Hervieu, H. Szymczak, K. Bärner, Phys. Rev. B **66**, 184424 (2002)
45. K.R. Poeppelmeier, M.E. Leonowicz, J.M. Longo, J. Solid State Chem. **44**, 89 (1982)
46. S. Nafis, J.A. Woollam, Z.S. Shan, D.J. Sellmyer, J. Appl. Phys. **70**, 6050 (1991)
47. F. Conde, C. Gomez-Polo, A. Hernando, J. Magn. Magn. Mater. **138**, 123 (1994)
48. K. Moorjani, J.M.D. Coey, *Magnetic Glasses, Methods and Phenomena*, Vol. 6 (Amsterdam, Elsevier, 1984), p. 184
49. N. Zhang, W. Ding, W. Zhong, D. Xing, Y. Du, Phys. Rev. B **56**, 8138 (1997)
50. N. Zhang, S. Zhang, W.P. Ding, W. Zhong, Y.W. Du, Solid State Comm. **107**, 417 (1998)
51. S. Lee, H.Y. Hwang, B.I. Shraiman, W.D. Ratcliff, S.W. Cheong, Phys. Rev. Lett. **82**, 4508 (1999)
52. H.L. Ju, C. Kwon, Q. Li, R.L. Greene, T. Venkatesan, Appl. Phys. Lett. **65**, 2108 (1994)